RSC Advances

PAPER

View Article Online
View Journal | View Issue

Cite this: *RSC Adv.*, 2020, **10**, 25200

Facile synthesis of a BCN nanofiber and its ultrafast adsorption performance

Junying Yu, †[ab] Tianjiao Hu,†[b] Ci Du,[b] Ye Zhang,[b] Zengyong Chu,[b] Yihe Li *[b] and Jing Cao*[a]

Received 29th February 2020
Accepted 24th June 2020

DOI: 10.1039/d0ra01938k

rsc.li/rsc-advances

Boron carbonitride (BCN) nanofibers with rapid and efficient adsorption performance were prepared by electrospinning technology. TEM, XRD, XPS and N_2 adsorption–desorption isotherms were performed to study the microstructure of the nanofibers. The results showed that the BCN fibers synthesized at 1000 °C (BCN-1000) have good crystallinity and high specific surface areas (403 m^2 g^{-1}). BCN-1000 nanofibers adsorb 70% of amino black 10B (AB-10B) within 10 minutes and reach adsorption equilibrium within 60 minutes. Compared with previous reports, it is found that the adsorption rate of BCN-1000 nanofibers to amino black (AB-10B) is much higher than that of other adsorbents. And BCN nanofibers exhibit a large adsorption capacity (625 mg g^{-1}). In addition, the process of AB-10B adsorption on BCN nanofibers was systematically investigated, which was in accordance with the pseudo-second-order kinetics model and Langmuir isotherm model.

Introduction

Dye, which has a high organic matter content and complex composition, is considered to be the most important pollutant in wastewater. It is harmful to human health when dyes are discharged into bodies of water.[1,2] Adsorption technology is a simple and effective purification method that has been widely used in the treatment of dyed wastewater.[3,4] Natural adsorbents, such as clay minerals, chitosan, and cyclodextrin have the advantages of low price, nontoxicity, abundant availability, excellent compatibility, and good biodegradability. However, the practical application of natural absorbents has been limited by several shortcomings. For example, clay has a natural negative charge that limits the adsorption capacity of acid dyes.[5] Dried chitosan has low mechanical strength and exhibits little deformation.[6] The cyclodextrin monomer is not hygroscopic.[7] In contrast, synthetic adsorbents have more active sites, larger surface areas and controlled pore structures, which lead to better adsorption properties than those of natural adsorbents.[8] In recent years, nanomaterials, such as carbon nanostructures, silicon nanostructures and magnetic nanomaterials, have attracted extensive attention due to their unique physical and chemical properties.[9,10] Belessi *et al.*[11] synthesized titanium dioxide nanoparticle adsorbents to remove the azo dye, reactive red 195 (RR195). At 30 °C, pH = 3.0 and 120 minutes, the maximum monolayer adsorption obtained by a Langmuir model was 87 mg g^{-1}. Chen *et al.*[12] prepared ECH-RB5 and ECH-3R nanoparticles of templated cross-linked chitosan for the removal of azo dyes using an imprinting process. At 30 °C, pH = 3.0 and 120 h, the maximum monolayer adsorptions obtained according to the Langmuir model were 5572 and 5392 mg g^{-1} for the dyes Remazol Black 5 (RB5) and Remazol Brilliant Orange 3R (3R), respectively. Ma *et al.*[13] synthesized alkali-activated carbon nanotubes for the removal of methyl orange (MO) and methylene blue (MB). Over 60 minutes, the adsorption capacity of the alkali-activated carbon nanotubes for MO and MB were 149 and 399 mg g^{-1}, respectively. Nanomaterials have a large adsorption capacity for dye; however, due to high production cost and slow adsorption speed, the adsorption efficiency of most nanomaterials is low. Therefore, it is a challenge to find a low-cost adsorbent that can quickly absorb dyes.

Boron carbonitride (BCN) is a novel, metal-free, synthetic material that has unique physical and chemical properties.[14] The hexagonal BCN (h-BCN) has a structure similar to hexagonal boron nitride (h-BN) and graphite.[15] The bandgap and conductive properties of h-BCN can be easily adjusted by controlling the composition.[16] Therefore, h-BCN has been widely used in electronic devices, supercapacitors, catalysts, adsorbents and other materials.[17–20] The reported synthesis methods mainly include magnetron sputtering,[21] chemical vapor deposition (CVD),[22] thermal solvents,[23] high temperatures and high pressures,[24] precursor pyrolysis,[25] and electrospinning.[26] Among these methods, electrospinning is a fast, simple and efficient fiber production process. Nanofibers prepared by electrospinning have a high specific surface area and are quite suitable for use as adsorption materials.[27] In

[a]*College of Chemistry, Xiangtan University, Xiangtan, Hunan, 411105, China. E-mail: yujunying2020@163.com; caojing8088@xtu.edu.cn*

[b]*College of Liberal Arts and Science, National University of Defense Technology, Changsha 410073, China. E-mail: tjhu@nudt.edu.cn; dc2006sg@126.com; zhangye8905@foxmail.com; chuzy@nudt.edu.cn; yhli@nudt.edu.cn*

† These authors contributed equally to this work.

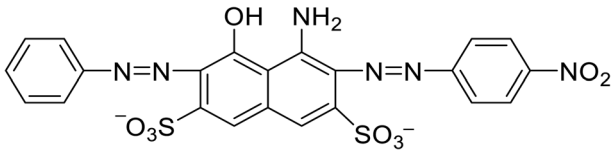

Fig. 1 The molecular structure of AB-10B.

addition, the adjustable valence band structure of BCN provides the possibility for dye degradation. Therefore, BCN nanofibers prepared by electrospinning technology are quite suitable for use as adsorption degradation materials. However, relevant research in this area is currently lacking.

AB-10B is an azo anion dye, the molecular formula is $C_{22}H_{14}N_6Na_2O_9S_2$, and the molecular structure is shown in Fig. 1. The dye is chemically stable and not biodegradable. Therefore, it is difficult to remove from water. In order to efficiently and quickly remove organic dye AB-10B from wastewater. In this investigation, through AB modified PAN fibers, NH_3 provides N element, BCN nanofibers were successfully prepared by electrospinning technology. The synthesized BCN nanofibers exhibited excellent adsorption performance for removing AB-10B dye. BCN nanofibers can quickly adsorb AB-10B, and the adsorption capacity reaches 625 mg g^{-1}. The facile, low-cost, effective synthesis of BCN nanofibers for the removal of AB-10B make this material a promising candidate for practical applications.

Materials and methods

Materials

Ammonia borane (AB) was obtained from Shanghai McLean Biotechnology Co., Ltd. *N*,*N*-Dimethylformamide (DMF) was purchased from Shanghai Qian shun Chemical Reagent Co., Ltd. Polyacrylonitrile (PAN) was obtained from Shenzhen Lute New Material Technology Co., Ltd. Amino black 10B (AB-10B) was bought from Shanghai Mclean Co., Ltd. All the reagents were analytically pure.

Preparation of the BCN nanofibers

5 g of PAN was weighed, dissolved in 45 g of DMF, and stirred at room temperature until completely dissolved to prepare 10% PAN/DMF solution. Then, 1.84 g of DMF was weighed and added to 8 g of the 10% PAN/DMF solution and stirred for until completely mixed. Next, weigh 0.16 g AB was added into this mixture and stirred until completely dissolved to make the spinning fluid. The spinning solution was drawn into a 5 mL syringe with a 0.8 mm diameter needle. A syringe pump was applied a constant flow rate of 1 mL h^{-1}. The working voltage was set to 15 kV. The distance between the needle and the iron ring collector was 10 cm.

After electrospinning, precursor fibers are placed in a horizontal tube furnace. Before heating, it takes about 30 minutes to exhaust the air in the furnace tube. Followed by high temperature calcination, in which the temperature rises from 30 °C to 500 °C, the cracking gas is N_2, when the temperature rises from 500 °C to 1000 °C, the flow rate is 400 mL min^{-1}, and the cracking gas is NH_3. Fig. 2 illustrates the whole fabrication process and heating procedure of BCN nanofibers. These obtained samples were named BCN-*x*, where *x* is the calcining temperature.

Characterizations of BCN nanofibers

X-ray diffraction (XRD) measurements were carried out on a Bruker D8 powder X-ray Cu Kα radiation diffractometer at 60 kV and 60 mA (Bruker, Germany). Transmission electron microscopy (TEM) was conducted using a Tecnai G2 F20 S-TWIN TMP (FEI Inc., U.S.). X-ray photoelectron spectroscopy (XPS) was carried out using a Thermo Scientific K-Alpha+ (Thermo Fisher Scientific Inc., U.S.). The surface functionality of BCN was studied using a Nicolet IS 10 FTIR spectrometer in the range of 400–4000 cm^{-1} (Thermo Fisher Scientific Inc., U.S.). The specific surface area of the samples was determined using the Brunauer–Emmett–Teller (BET) equation (JW-BK200C, Beijing JWGB Sci. & Tech. Co., Ltd). Thermogravimetric analysis (TGA) of the precursor was conducted using a Shimadzu TGA 50 (Shimadzu, Inc., Japan) at a heating rate of 10 °C min^{-1} from 30 °C to 1000 °C under nitrogen. The adsorption capacity of the nanofibers was

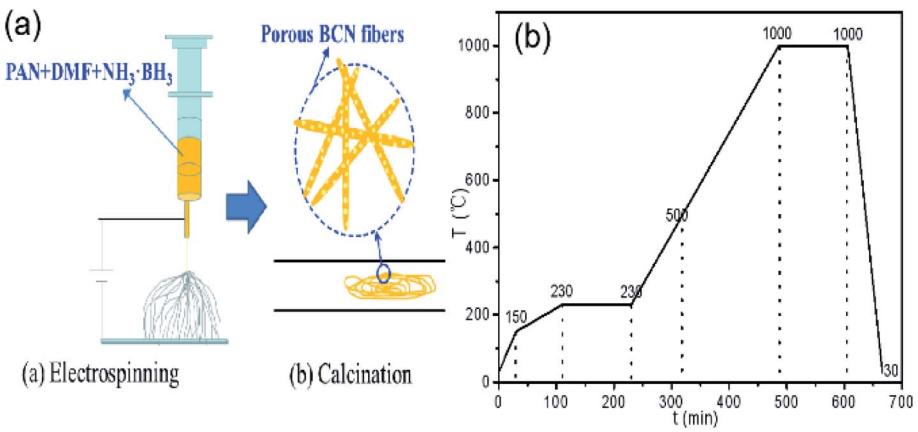

Fig. 2 Fabrication process (a) and heating procedure (b) of BCN nanofibers (30–500 °C in N_2, 500–1000 °C in NH_3).

determined using a UV-vis spectrophotometer (760CRT, INEAA, CN) at a wavelength of 620 nm.

Evaluation of adsorption performance

A certain amount of adsorbent was added to a certain concentration of dye in a 50 mL volume. These mixtures were allowed to adsorb at room temperature for a certain amount of time. After the adsorption was completed, the absorbance of AB-10B at the maximum absorption wavelength was measured by a UV-vis spectrophotometer. The adsorption capacity, q_e (mg g^{-1}), and removal rate, φ_e (%), of the dye were then be calculated according to the following formulas:

Adsorption capacity:

$$q_e = \frac{(C_0 - C_e) \times V}{M}$$

Removal rate:

$$\varphi_e = \frac{(C_0 - C_e)}{C_0} \times 100\%$$

the C_0 (mg L^{-1}) and C_e (mg L^{-1}) are the initial concentration of the dye solution and the concentration at a given time after adsorption, respectively; V (mL) is the initial volume of the dye solution; m (g) is the mass of the added adsorbent.

Effect of the adsorbent dose on adsorption performance

A solution of AB-10B 200 mg L^{-1} was prepared. BCN-1000 was added to 50 mL of the dye solution in amounts that varied from 0.005 g to 0.02 g. These mixtures were allowed to adsorb for 60 min at room temperature. The absorbance at the maximum wavelength of AB-10B was measured and used to calculate the amount of adsorption.

Effect of the initial concentration of the solution on the adsorption properties

Solutions of 200–500 mg L^{-1} dyes solution were prepared. Then, 0.02 g BCN-1000 was added into a series of different concentrations of dye solutions (50 mL each) to adsorb for 5–60 min at room temperature. The corresponding second order dynamic models were calculated, and the corresponding isotherm models were fitted to the obtained data.

Result and discussion

Preparation and characterization

Fig. 3 shows optical images, SEM, TEM, HRTEM and SAED images of the BCN-1000 nanofibers. Fig. 3a shows SEM image of BCN precursor fibers. It can be seen from the SEM image that the surface of the BCN precursor fibers are smooth and the diameter are uniform. Fig. 3b shows SEM image of the BCN nanofibers. As can be seen from the figure, after carbonization BCN nanofibers are further cross-linked. The optical images (inset in Fig. 3b) show that the BCN nanofibers are pale yellow. In Fig. 3c, the BCN nanofibers have structures with diameters ranging from 50–90 nm. The interplanar distance of the graphitized crystal structure (002) of the BCN nanofibers is approximately 0.34 nm (inset in Fig. 3d).[28] The SAED images (inset in Fig. 3d) indicate that the BCN samples are

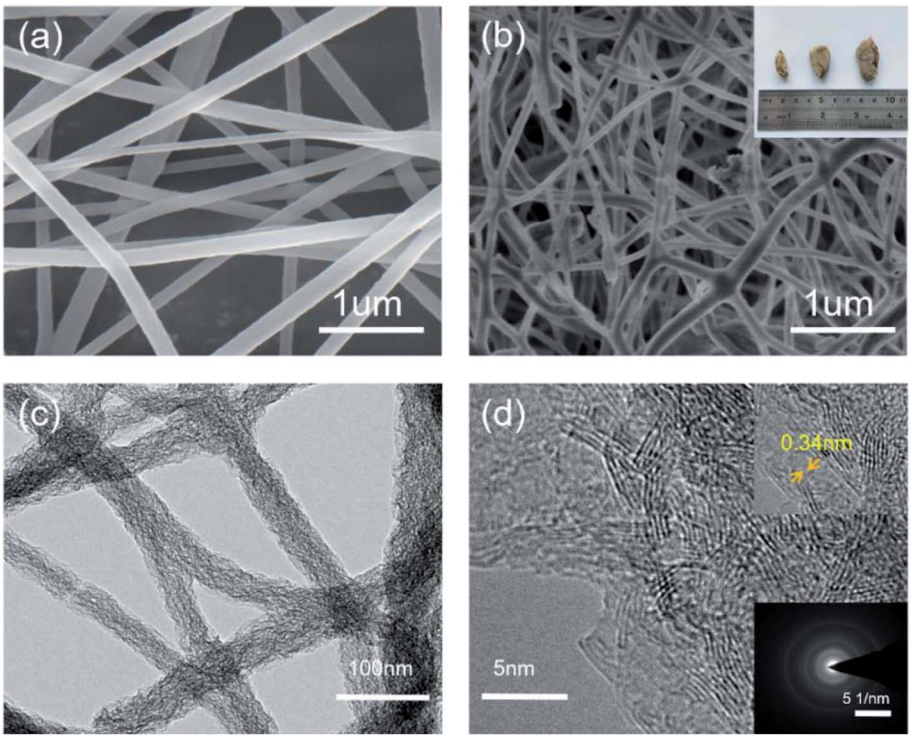

Fig. 3 Surface morphology of BCN-1000. (a) SEM image of BCN precursor fibers (b) SEM image of BCN (insets: optical image of BCN) (c) TEM image of BCN, and (d) HRTEM image of the BCN sample (insets: SAED image of BCN).

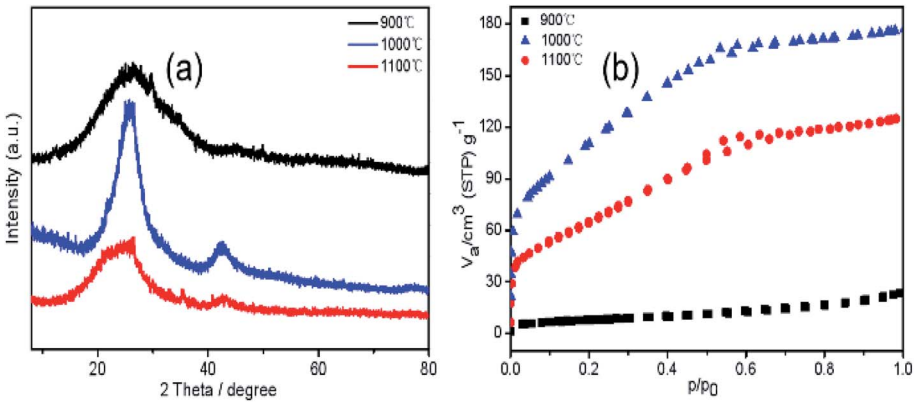

Fig. 4 XRD patterns (a) and N_2 adsorption/desorption isotherms (b) of BCN at different temperatures.

polycrystalline, which may suggest that C mainly forms at grain boundary of the BN domain.[14]

Fig. 4a shows the XRD patterns of the samples pyrolyzed at different temperatures. The peaks at 25.4° and 42.5° can be ascribed to the diffraction of the (002) and (100) planes of the graphitic crystal structure of h-BN.[28] The interlayer spacing corresponding to the (002) crystal plane diffraction peaks, according to Bragg's law, is 0.33 nm. The crystallinity of the sample pyrolyzed at 1000 °C is most pronounced. According to the nitrogen adsorption–desorption isotherms of the samples pyrolyzed at different temperatures shown in Fig. 4b, the specific surface area of the BCN-900, BCN-1000, and BCN-1100 samples are 27, 403, and 243 $m^2\ g^{-1}$, respectively. It is speculated that when the pyrolysis temperature is increased from 900 °C to 1000 °C, the structure of the fibers is rearranged to generate a lot of small molecules. The escape of these small molecules leads to a significant increase in the fiber porosity. However, when the temperature is further increased to 1100 °C, the skeleton of the sample collapses, and the specific surface area decreases.

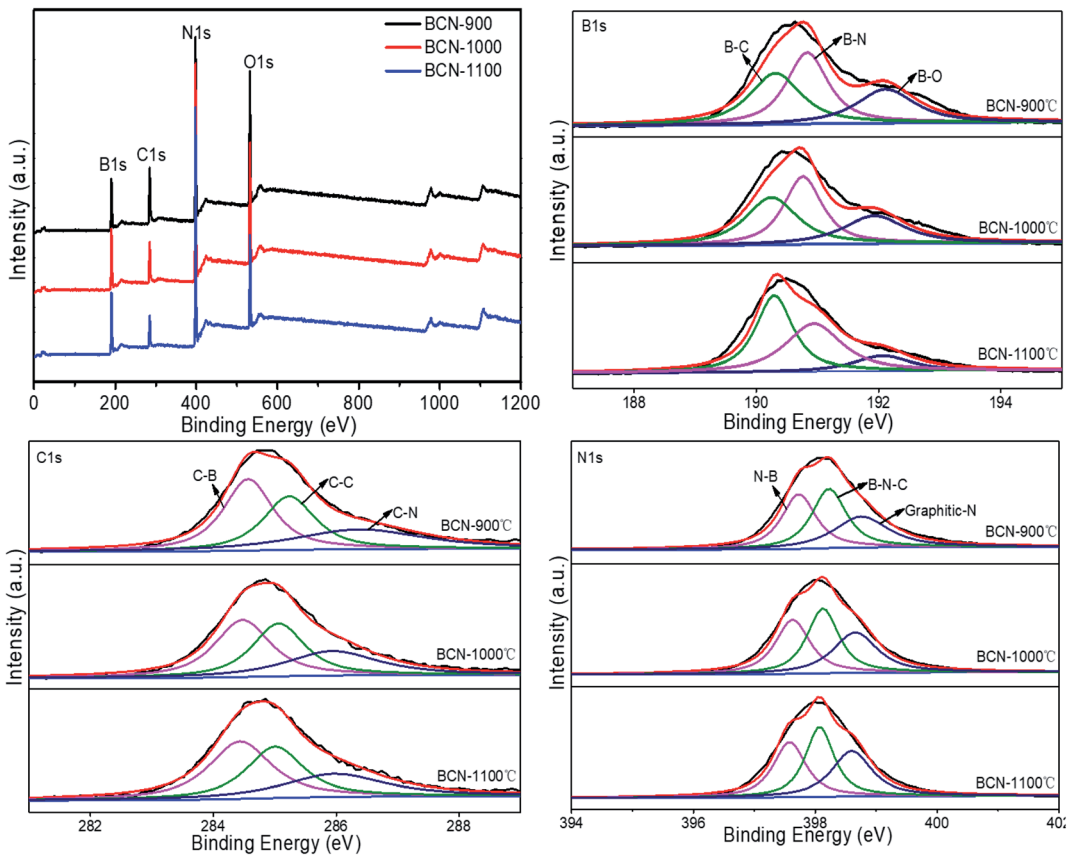

Fig. 5 XPS survey and hight-resolved spectra of the BCN.

Table 1 Elemental analysis of different temperature of BCN

Sample	B 1s			C 1s			N 1s			O 1s
BCN-900	1.00	B–N	1.00	1.00	C–B	1.00	1.00	N–B	0.98	1.00
		B–C	0.96		C–C	0.95		B–N–C	1.00	
		B–O	0.87		C–N	0.92		Graphitic N	0.95	
BCN-1000	1.11	B–N	1.00	0.70	C–B	1.00	1.11	N–B	0.97	0.86
		B–C	0.98		C–C	0.98		B–N–C	1.00	
		B–O	0.87		C–N	0.95		Graphitic N	0.95	
BCN-1100	1.16	B–N	0.96	0.56	C–B	1.00	1.19	N–B	0.96	0.73
		B–C	1.00		C–C	0.97		B–N–C	1.00	
		B–O	0.69		C–N	0.94		Graphitic N	0.97	

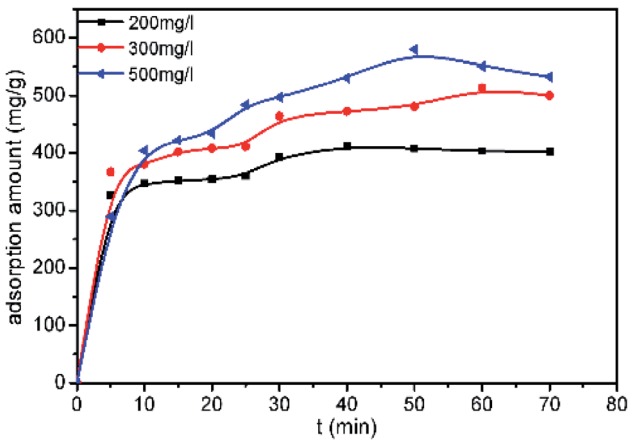

Fig. 6 Time profiles of AB-10B adsorption on the BCN-1000.

A typical XPS spectrum of the BCN nanofibers is shown in Fig. 5. The full range scan of the sample show that it contains B, C, N, and O. AB is easily hydrolyzed in air, which introduces oxygen. In the B 1s spectrum, a peak at 190.8 eV can be attributed to the B–N bond. Since the electronegativity of C is less than that of N, the peak at 190.3 eV can be attributed to the B–C bond, while the peak at 192.0 eV corresponds to the B–O bond. In the C 1s spectrum, the peak at 285.2 eV corresponds to a C–C bond. The peaks at 284.5 eV on the low energy side and 286.4 eV on the high energy side are assigned to the C–B bond and C–N bond, respectively. The N 1s spectrum exhibits three peaks located at 397.7 eV, 398.2 eV and 398.7 eV, which correspond to the N–B bond, B–N–C bonds and graphitic-N bonds, respectively. Thus, the XPS analysis shows that carbon exists in the h-BN lattice.[29]

As seen in Table 1, with increasing pyrolysis temperature, the contents of B and N gradually increase, while the contents of C and O gradually decrease. This result occurs because with increasing pyrolysis temperature, the B–O bond is broken, therefore, the content of O decreases. Furthermore, non-carbon atoms in PAN fibers are discharged through various gas forms with increasing temperature, and carbon atoms are enriched; as the temperature rises further, when ammonia gas is introduced, the N in the NH_3 molecule continuously reacts with B in fibers to form B–N bonds, which gradually increases contents of B and N. However, the B–O bond is relatively stable, so it cannot completely bind to the N in NH_3. Therefore, NH_3 reacts with C in the fibers to produce a decarburization effect, which greatly reduces the C content in the fibers. In the B 1s, C 1s, and N 1s spectra, there are three kinds of bonds. That is, any one of the B, C, and N elements is chemically bonded to the other two elements. Therefore, B, C, and N are present at the atomic level, rather than as a simple mixture of h-BN and graphite.

It can be seen from the XRD patterns from the different temperatures that the crystallinity of samples is best at 1000 °C. The nitrogen adsorption/desorption isotherm test results show that at 1000 °C, BCN-1000 have high specific surface area (403 $m^2\ g^{-1}$). Therefore, BCN nanofibers were selected for the performance test at 1000 °C.

AB-10B adsorption property

Fig. 6 shows the effect of contact time on the dye adsorption in solutions at different initial concentrations with a fixed

Table 2 Adsorption capacity of AB-10B on various adsorbents and the time required to reach equilibrium

Adsorbent	q_m (mg g^{-1})	Time (t)	References
A: BCN nanofibers	625	60	This paper
B: polyethyleneimine modified bentonite	264.5	60	31
C: crosslinked quaternized chitosan/bentonite composite	990.1	300	32
D: Zr(IV) surface-immobilized cross-linked chitosan/bentonite composite	418.4	300	33
E: porous chitosan doped with graphene oxide	573.47	100	34
F: polyaniline/iron oxide	56	200	35
G: bentonite modified by allylamine polymer	144.08	120	36
H: jackfruit leaf powder	3.7	240	37
I: protonated cross-linked chitosan	18.8	60	38

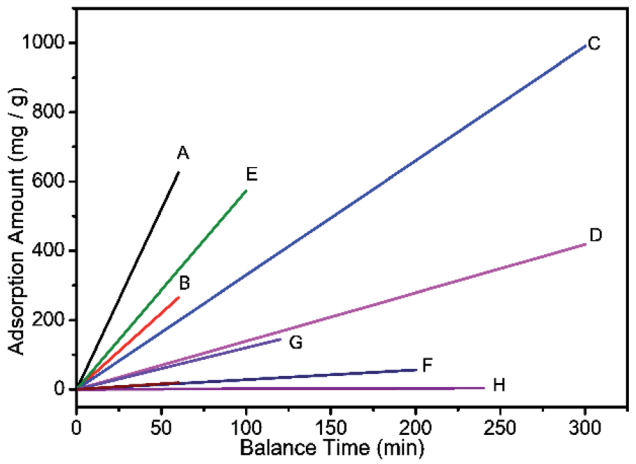

Fig. 7 Diagram of equilibrium time and maximum adsorption capacity (correspond Table 2).

Table 3 Adsorption parameter of kinetics for the adsorption of AB-10B on BCN-1000

	Pseudo-first-model		Pseudo-second-model	
C (mg L^{-1})	k_1 (min^{-1})	R^2	k_2 (min^{-1})	R^2
200	0.007427	0.7119	0.00252	0.98985
300	0.04888	0.45929	0.00198	0.99183
500	0.05541	0.92824	0.00168	0.99298

adsorbent dose of 0.02 g. The results show that the adsorption equilibrium capacity increases with increasing initial concentration. When the initial concentration is 500 mg L^{-1}, the maximum adsorption equilibrium capacity of the sample reaches 528 mg g^{-1}. The adsorption process can be divided into two stages. The first stage is the initial rapid adsorption stage, which lasts 10 minutes. In this stage, 70% of AB-10B was adsorbed. The main reason for rapid adsorption is that the high surface area of the nanofibers provides sufficient vacant adsorption sites. In the second stage, which is denoted as the slow adsorption stage, the adsorption rate slows as the empty adsorption sites become occupied. The number of adsorption sites and diffusion resistance may be the main factors limiting the adsorption rate.[30]

BCN-1000 can adsorb 70% of AB-10B within 10 minutes and reach adsorption equilibrium within 60 minutes. To the best of our knowledge, this rate is relatively fast when compared to previous reports. Table 2 lists the adsorption capacity of AB-10B for various adsorbents and the time required to reach equilibrium.

Fig. 7 shows a diagram of equilibrium time and maximum adsorption capacity (corresponding to Table 2). The data show that the speed of AB-10B adsorption by the BCN nanofibers is the fastest and is much faster than that of other adsorption materials.

The absorption kinetics of AB-10B on BCN fibers were further studied by using the pseudo-first-order and pseudo-second-order kinetic models. The formulas used in these models are defined as:

$$\ln(q_e - q_t) = \ln q_e - k_1 t \quad (1)$$

$$\frac{t}{q_t} = \frac{1}{k_2 q_e^2} + \frac{t}{q_t} \quad (2)$$

Table 4 Adsorption parameter of isotherm for the adsorption of AB-10B on BCN-1000

	Langmuir			Freundlich		
Sample	q_m (mg g^{-1})	b	R^2	k_f	n	R^2
AB	625.114	0.0690	0.98768	120.590	3.245	0.87166

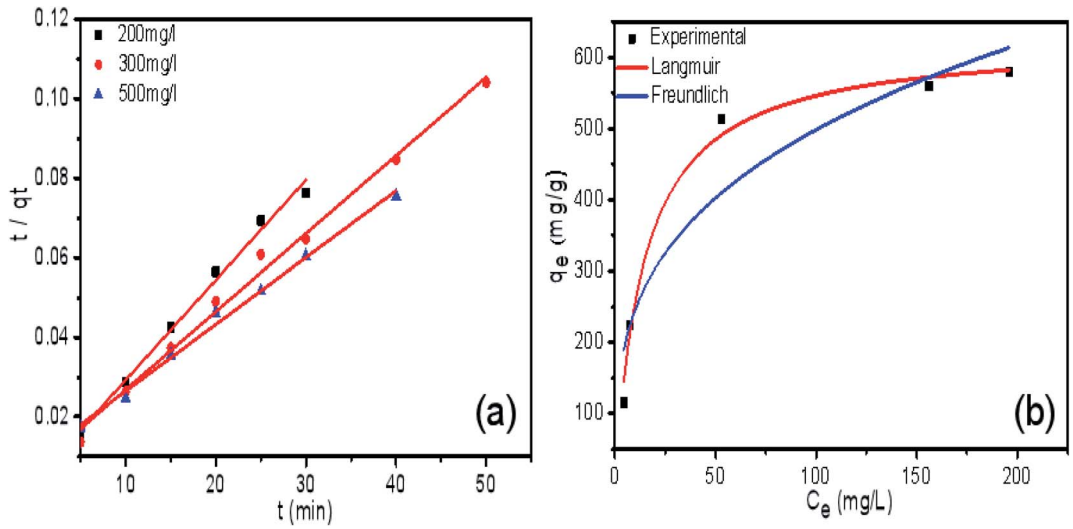

Fig. 8 The pseudo-second-order kinetics plots (a) and adsorption isotherm curves (b) of AB-10B adsorption on BCN-1000 nanofibers.

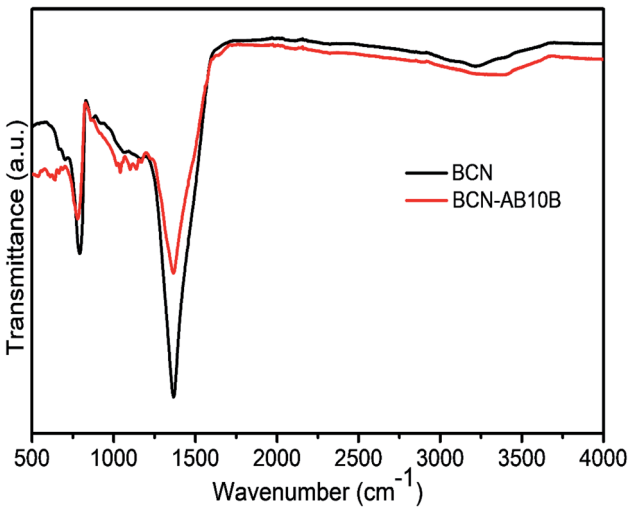

Fig. 9 FTIR spectra of BCN-1000 before and after adsorption.

the q_e (mg g^{-1}) represents the adsorption amount at equilibrium, q_t (mg g^{-1}) is adsorption capacity at time t (min). The k_1 is the pseudo-first-order (min^{-1}) rate constant, k_2 is rate constant of the pseudo-second-order (g mg^{-1} min^{-1}). Table 3 gives the kinetic parameters and their correlation coefficients (R^2).

As seen in Fig. 8a, all the experimental data are well represented by the pseudo-second-order model because the correlation coefficient is very high (R^2 > 0.99). This correlation indicates that the adsorption process of AB-10B on the BCN nanofibers obeys the pseudo-second-order model. The adsorption isotherm curves of AB-10B adsorption on BCN nanofibers are shown in Fig. 8b. The adsorption process is described by Langmuir (eqn (3)) and Freundlich (eqn (4)) isotherms:

$$q_e = \frac{q_m b C_e}{1 + b C_e} \quad (3)$$

$$q_e = k_f C_e^{\frac{1}{n}} \quad (4)$$

the q_m (mg g^{-1}) is the maximum adsorption amount of dye, b is the equilibrium constant (L mg^{-1}), the k_f represents the level of adsorption amount, and n represents the adsorption intensity.

The related parameters and the correlation coefficients (R^2) are listed in Table 4. The adsorption data agree better with the Langmuir model (R^2 = 0.988) than with the Freundlich model (R^2 = 0.872), which describes a monolayer adsorption of the BCN fibers. According to the Langmuir model, the maximum adsorption capacity of AB-10B to BCN was 625.114 mg^{-1}.

To further study the adsorption mechanism, FTIR studies were performed on AB-10B-loaded adsorbents. The FTIR spectrum shown in Fig. 9 indicates that the internal structure did not change before and after adsorption, which indicates that the adsorption process is a physical adsorption. It is also noted in Fig. 9 that the band intensity of B–N decreases after adsorption of AB-10B onto BCN. This indicates that favorable adsorption occurs through polar B–N bonds.[39]

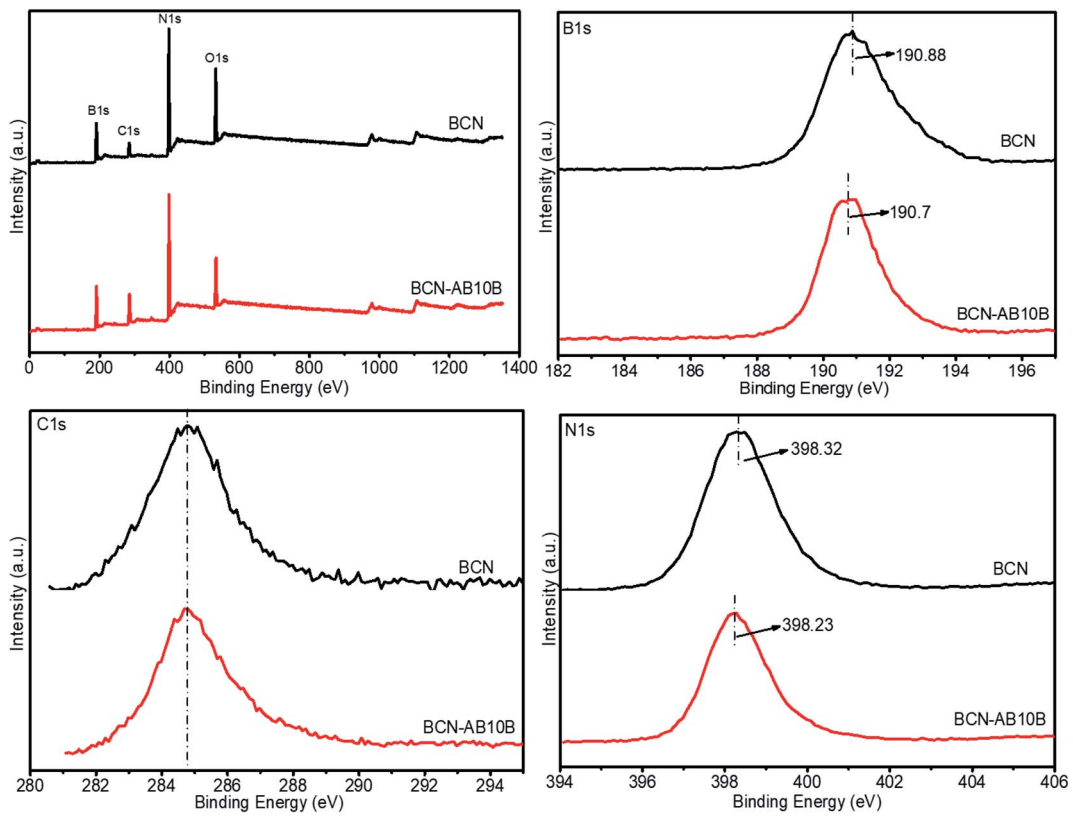

Fig. 10 XPS of BCN-1000 before and after adsorption.

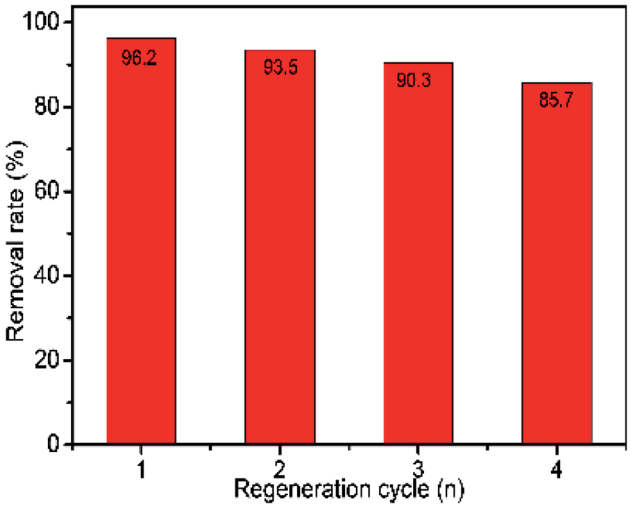

Fig. 11 Recyclability of regenerated BCN-1000 for the adsorption of AB-10B.

The adsorption mechanism of BCN and BCN after adsorption of AB-10B, *i.e.* BCN-AB10B, were studied using XPS. The survey spectra spectrum shown in Fig. 10 indicates that samples contain B, C, N and O. The high-resolution spectra of C (1s), B (1s), and N (1s) provide details of the binding information of BCN nanofibers and AB-10B adsorbed BCN nanofibers. For boron (1s), we observed that before and after adsorption, a peak shifted from 190.88 eV (BCN) to 190.7 eV (BCN-AB10B). For nitrogen (1s), we observed that before and after adsorption, a peak shifted from 398.32 eV (BCN) to 398.23 eV (BCN-AB10B). The XPS spectra with respect to boron and nitrogen peak shifts indicates that polar B–N bonds has good adsorption, which is consistent with FTIR analysis in Fig. 9.

The reuse of the adsorbent can greatly reduce the cost of adsorption, and enables green chemistry.[40] Therefore, it is necessary to study the cyclic performance of BCN nanofiber adsorbents. Regeneration of nanofibers was carried out using anhydrous ethanol. As shown in Fig. 11, after four adsorption and desorption cycles, the relative ratio of the adsorption capacity was found to be 85.7% for BCN nanofibers. These results indicate that BCN fibers have good recycling performance. In practical applications, recycling of the adsorbent can be achieved by regeneration using ethanol.

Conclusion

In summary, we successfully prepared BCN nanofibers by electrospinning and pyrolysis using a mixture of PAN and AB. It shows good adsorption capacity and high adsorption rate for azo anionic dye AB-10B, which is superior to many other adsorbents reported in the literature. This result was mainly attributed to the high specific surface area of BCN nanofibers (403 $m^2 g^{-1}$) and polar B–N bonds. In addition, BCN nanofibers have good adsorption and regeneration properties for AB-10B. BCN nanofibers have broad application prospects in wastewater treatment because of their advantages, including simple preparation, low cost and strong adsorption.

Conflicts of interest

There are no conflicts to declare.

References

1 N. B. Singh, G. Nagpal, S. Agrawal and Rachna, *Environ. Technol. Innov.*, 2018, **11**, 187.
2 Momina, S. Mohammad and S. Isamil, *J. Water Process Eng.*, 2020, **34**, 101155.
3 Y. Zhou, J. Lu, Y. Zhou and Y. Liu, *Environ. Pollut.*, 2019, **252**, 352.
4 H. Lyu, K. Hu, J. Fan, Y. Ling, Z. Xie and J. Li, *Appl. Surf. Sci.*, 2020, **500**, 144037.
5 S. Arellano-Cárdenas, S. López-Cortez, M. Cornejo-Mazón and J. C. Mares-Gutiérrez, *Appl. Surf. Sci.*, 2013, **280**, 74.
6 N. V. Hoa, T. T. Khong, T. T. Hoang Quyen and T. Si Trung, *J. Water Process Eng.*, 2016, **9**, 170.
7 A. Mohammadi and P. Veisi, *J. Environ. Chem. Eng.*, 2018, **6**, 4634.
8 L. Y. Jun, N. M. Mubarak, M. J. Yee, L. S. Yon, C. H. Bing, M. Khalid and E. C. Abdullah, *J. Ind. Eng. Chem.*, 2018, **67**, 175.
9 D. Talbot, S. Abramson, N. Griffete and A. Bée, *J. Water Process Eng.*, 2018, **25**, 301.
10 A. A. Basheer, *J. Mol. Liq.*, 2018, **261**, 583.
11 V. Belessi, G. Romanos, N. Boukos, D. Lambropoulou and C. Trapalis, *J. Hazard. Mater.*, 2009, **170**, 836.
12 C. Y. Chen, J. C. Chang and A. H. Chen, *J. Hazard. Mater.*, 2011, **185**, 430.
13 J. Ma, F. Yu, L. Zhou, L. Jin, M. Yang, J. Luan, Y. Tang, H. Fan, Z. Yuan and J. Chen, *ACS Appl. Mater. Interfaces*, 2012, **4**, 5749.
14 F. Guo, P. Yang, Z. Pan, X.-N. Cao, Z. Xie and X. Wang, *Heterog. Catal.*, 2017, **56**, 8231.
15 Y. Fang and X. Wang, *Angew. Chem.*, 2017, **56**, 15506.
16 M. D. Gilan and R. Chegel, *Phys. E*, 2018, **97**, 177.
17 L. Liao, K. Liu, W. Wang, X. Bai, E. Wang, Y. Liu, J. Li and C. Liu, *J. Am. Chem. Soc.*, 2007, **129**, 9562.
18 D. Chen, X. Hu, Y. Huang, Y. Qian and D. Li, *Mater. Lett.*, 2019, **246**, 28.
19 L. Wang, C. Wang, Z. Zhang, J. Wu, R. Ding and B. Lv, *Appl. Surf. Sci.*, 2017, **422**, 574.
20 Q. Hao, Y. Song, Z. Mo, S. Mishra, J. Pang, Y. Liu, J. Lian, J. Wu, S. Yuan, H. Xu and H. Li, *ACS Sustainable Chem. Eng.*, 2019, **7**, 3234.
21 A. Prakash, K. B. Sundaram and A. D. Campiglia, *Mater. Lett.*, 2016, **183**, 355.
22 J. Lü, H. Li, P. Zhu, X. Lü and Y. Li, *Appl. Surf. Sci.*, 2011, **257**, 4963.
23 J. Li, N. Lei, H. Hao and J. Zhou, *Chem. Phys. Lett.*, 2017, **672**, 99.
24 P. Bhattacharyya, S. Sahoo, A. H. Seikh, S. M. A. K. Mohammed, A. Sarkar and N. Alharthi, *Diamond Relat. Mater.*, 2019, **92**, 235–241.
25 T. Zhang, S. F. Zeng and G. Wen, *Mater. Lett.*, 2014, **132**, 277.
26 B. H. Kim and K. S. Yang, *Electrochim. Acta*, 2013, **88**, 597.

27 H. Hu, S. Wageh, A. A. Al-Ghamdi, S. Yang, Z. Tian, B. Cheng and W. Ho, *Appl. Surf. Sci.*, 2020, **511**, 145570.
28 L. Chen, M. Zhou, Z. Luo, M. Wakeel, A. M. Asiri and X. Wang, *Appl. Catal., B*, 2019, **241**, 46.
29 C. Huang, C. Chen, M. Zhang, L. Lin, X. Ye, S. Lin, M. Antonietti and X. Wang, *Nat. Commun.*, 2015, **6**, 7698.
30 T. Lou, X. Yan and X. Wang, *Int. J. Biol. Macromol.*, 2019, **135**, 919.
31 S. Du, L. Wang, N. Xue, M. Pei, W. Sui and W. Guo, *J. Solid State Chem.*, 2017, **252**, 152.
32 L. Zhang, P. Hu, J. Wang and R. Huang, *Int. J. Biol. Macromol.*, 2016, **93**, 217.
33 L. Zhang, P. Hu, J. Wang and R. Huang, *Appl. Surf. Sci.*, 2016, **369**, 558.
34 Y. Wang, G. Xia, C. Wu, J. Sun, R. Song and W. Huang, *Carbohydr. Polym.*, 2015, **115**, 686.
35 R. Ahmad and R. Kumar, *J. Mol. Liq.*, 2017, **241**, 1091.
36 W. Guo, T. Xia, M. Pei, Y. Du and L. Wang, *Polymers*, 2019, **11**, 502.
37 A. K. Ojha and V. K. Bulasara, *J. Environ. Chem. Eng.*, 2015, **3**, 2647.
38 Q. Liu, B. C. Yang, J. Huo and R. H. Huang, *J. Mater. Sci. Eng.*, 2012, **140**, 1673.
39 S. Wang, F. Jia, P. Kumar, A. Zhou, L. Hu, X. Shao, X. Wang, Y. Sun, G. Yin and B. Liu, *Colloids Surf., A*, 2020, **598**, 124865.
40 B. Wang, Q. Zhang, G. Xiong, F. Ding, Y. He, B. Ren, L. You, X. Fan and C. Hardacre, *Chem. Eng. J.*, 2019, **366**, 404.